GOSPODARKA SUROWCAMI MINERALNYMI – MINERAL RESOURCES MANAGEMENT

2025 Volume 41 Issue 1 Pages 83–105

DOI: 10.24425/gsm.2025.153170

ALIM H. BARAN[1]

Geochemistry and fluid-inclusion microthermometry of the Orenagil barite deposit, Türkiye

Introduction

Ba and SO_4 are the main components of barite. The most important source of Ba is the crust, while the primary source of SO_4 is seawater. The sedimentary exhalative (Sedex) and Mississippi Valley-type (MVT) barite deposits are the most common types of barite formations in the world. Sedex barite deposits tend to be large Paleozoic reserves (Derakhshi et al. 2020) that are compatible with the host rocks (syngenetic), while MVT deposits are smaller, younger (mostly Mesozoic), and incompatible (epigenetic) mineralization. Although MVT reserves are not as large as sedex-type reserves, they constitute 25% of the world's lead and zinc reserves (Paradis et al. 2007).

There is a link between sex and MVT reserves in that each side bed has an MVT extension. It is thought that tectonic activity affecting sedex deposits remobilized barite into upper layers, resulting in the formation of younger, epigenetic MVT deposits. Hydrothermal

✉ Corresponding Author: Alim H. Baran; e-mail: hacialim.baran@batman.edu.tr

[1] Department of Geological Engineering, Batman University, Batman, 45320 Türkiye;
ORCID iD: 0000-0003-4859-8446; e-mail: hacialim.baran@batman.edu.tr

barite precipitation occurs as a result of the mixture of Ba-rich hydrothermal fluids with seawater near the seafloor while they rise through faults or fractures (Asl et al. 2015). Since the main components of these barites come from different sources, their geochemical properties indicate two different sources.

Subduction zones are geological environments that house mineral deposits of economic value, contribute to the shape of the Earth's crust, and cause powerful and dangerous earthquakes. The Bitlis–Zagros suture belt is a developed tectonic structure with collisions in the Arabian platform's Torid block and early-mid-Miocene, and the rocks surfacing

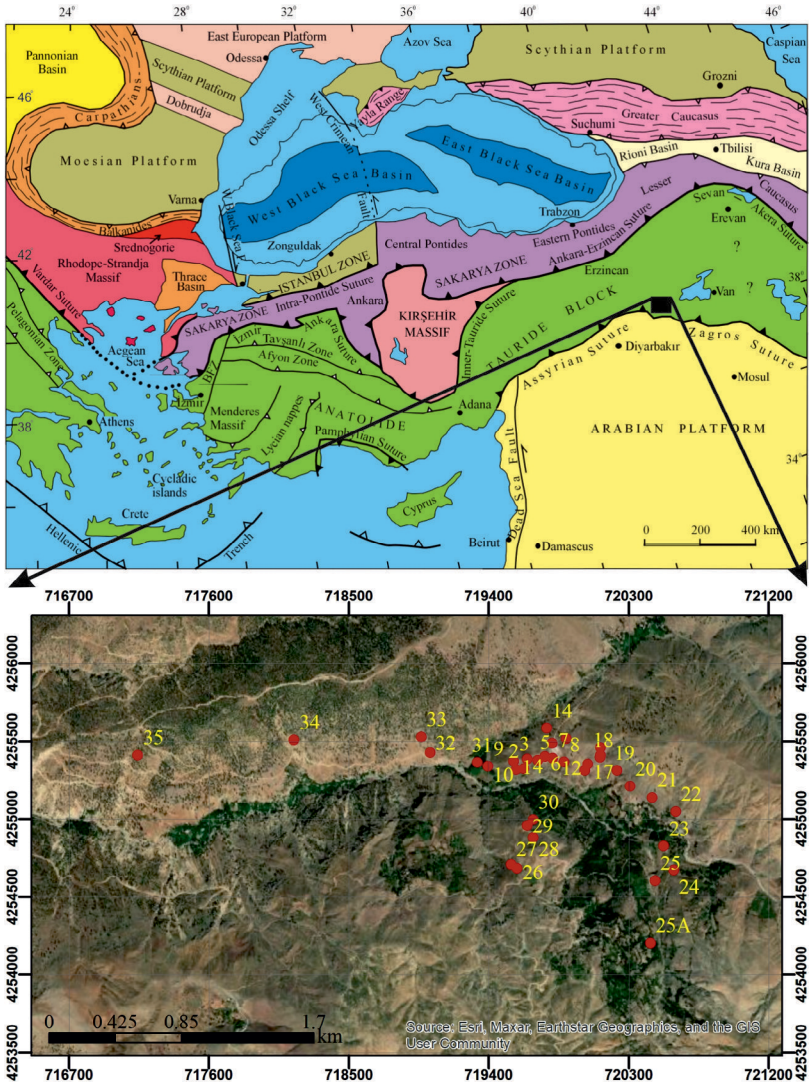

Fig. 1. Tectonic location of the study area (Okay 2008) and sampling map

Rys. 1. Położenie tektoniczne obszaru badań (Okay 2008) i mapa poboru prób

throughout this belt host many mineralizations of economic value. The Maden deposit (Cyprus-type volcanogenic massive sulfide deposit) observed in the Maden complex (Middle Eocene) (Şaşmaz et al. 2014; Çiftçi 2019), the Madenkoy deposit observed in Eocene sediments and pillow lavas (Akıncı 2009; Akkoca and Çelebi 2018; Farmer 2019), and the carbonate-hosted lead-zinc deposits in Hakkari (Santoro et al. 2013; Hanilçi et al. 2016, 2017, 2018, 2019) have all been studied by many researchers.

There are approximately 100 barite deposits investigated in the Iranian part of the Bitlis–Zagros suture belt and the formation of barites varies in age from late Cambrian to Miocene (Ghorbani 2013). Barites are generally observed as space fillings, veins, and lenses in carbonate rocks. (Zarasvandi et al. 2014; Asl et al. 2015). Mineralization is accompanied by sulfide minerals and Fe and Mn oxides (Zarasvandi et al. 2014; Ehya and Mazraei 2017; Hormozi et al. 2023). The formations representing the Zagros part of the belt were generally formed in the seawater and hydrothermal fluid mixing conditions. Barites located in the extension of the belt in Türkiye have probably not yet been discovered or studied in detail. No other study has been found other than the study conducted by Kumral (2010).

The study area is located northeast of Batman, Türkiye, north of the Bitlis suture zone (Figure 1). Göncüoğlu and Turhan (1985) suggested the existence of a large-scale geosyncline with its south wing in Batman and north wing in Mus. Therefore, Mus and Batman are similar in terms of both geological environments and observed geological units. Kumral (2010), in his study on barite mineralization in the Mus region, mentioned the existence of two types of mineralization showing sedex and MVT properties.

REE geochemistry and fluid inclusions are useful methods that are frequently used to determine the formation environments of barite deposits and the origin of the solution that caused their formation (Kato 1999; Zarasvandi et al. 2014; Alaminia and Sharifi 2018; Babaei and Ganji 2018; Hormozi et al. 2023). Within the scope of this study, the geological and petrographic characteristics of the Örenagil barite mineralization were determined, and its origin and formation environment were evaluated along with REE geochemistry and fluid inclusions.

1. Regional geology

As a result of the collision of the upcoming parts of the Bitlis-Zagros suture, the residual sea in Eastern Anatolia was closed at the end of the Early Miocene (Yılmaz et al. 1993). The continuation of the approach initiated crustal shortening and thickening during orogenesis and thus caused the rise of the Eastern Anatolian-Iranian plateau. The crust started to thicken as a result of the north-south compression deformation. This event initiated the widespread volcanic activity observed on the Turkish-Iranian high plateau (Yılmaz et al. 1987).

The region consists of three tectonostratigraphic units: Bitlis Metamorphic Belt, Sliced Belt, and Autochthon Belt, which are very different in terms of sedimentation environment,

metamorphism, magmatism, and age (Göncüoğlu and Turhan 1985). Bitlis Massif is an important metamorphic complex that surrounds Muş-Van-Bitlis and Siirt provinces and hosts economically important formations in Eastern Anatolia. The complex consists of the pre-Devonian Hizan group, the Devonian – Middle-Late Triassic Aged Mutki group, the Guleman ophiolite, the Late Maastrichtian Kinzu flysch and the Middle-Late Eocene non--metamorphic Kizilagac formation.

1.1. Geology of the study area

In the study area, the Meydan Formation, Cirrik Limestone, Malato Limestone, Tutu Formation, and Kizilagac Formation were observed (Figure 2, 3). The unit that has the widest spread in the study area and hosts the mineralization is the Meydan formation; the contact with the overlying units is tectonic (Figure 2).

Meydan Formation (Devonian) consists of schist (chlorite schist, sericite schist)--quartzite-recrystallized limestone alternating. Cirrik limestone consists of gray-black colored, medium-thick bedded, fossil-tracked recrystallized limestone containing yellow--gray colored calc-schist, graphite schist, and quartzite intermediates. Malato limestone consists of yellow, gray, and colored recrystallized limestone and intercalated pink-yellow calc-schists. Tutu formation starts with gray-colored, thick-bedded limestone at the bottom. It runs to top with yellow-green calc-schist and shale interlayered, medium-thin-bedded limestone. In the upper part of the unit, yellow-green colored metatuff, metaagglomerate, and metabasic rocks are exposed. There is red sandstone, green-red micrite, radiolarite, red-black agglomerate, and tuff banded calcarenite in combination with metabasic rocks. It is thought that the age of pelagic and volcanosedimanter rocks forming the upper part of the sequence reaches up to the Upper Cretaceous (Boray 1973). Kizilagac formation consists of grey-red color pebbles and light grey, medium-thick added, locally clayey limestone.

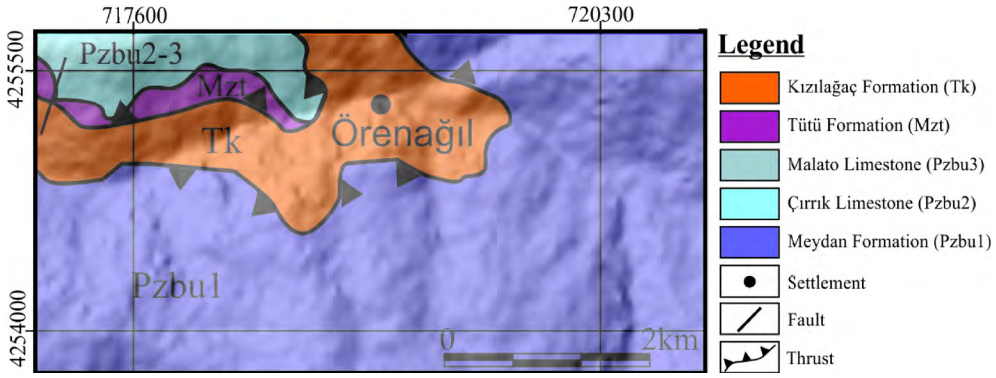

Fig. 2. Geological map of the study area (Göncüoğlu and Turhan 1985)

Rys. 2. Mapa geologiczna obszaru badań

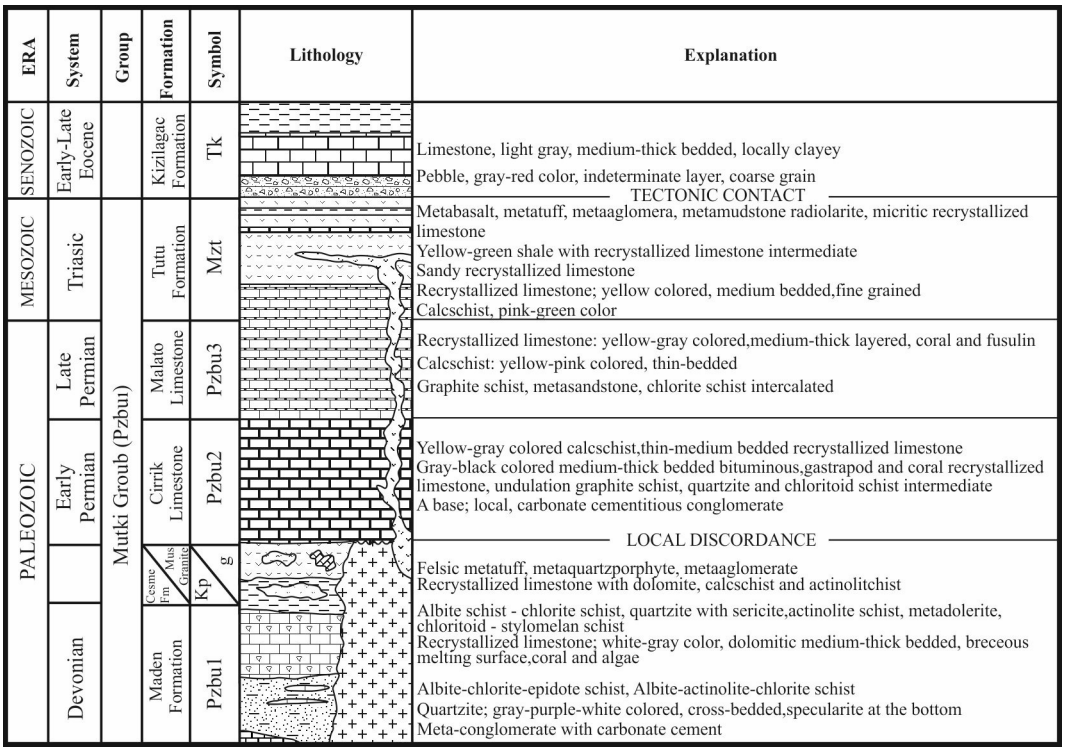

Fig. 3. Generalized column section of the region (Göncüoğlu and Turhan 1985)

Rys. 3. Uogólniony przekrój kolumnowy regionu

2. Data and method

The samples taken from the field were prepared for chemical analysis, and thin sections and polished samples were taken in the Batman University Geological Engineering Department Sample Preparation Laboratory. Chemical analyses of 30 samples were measured at Istanbul Technical University Geological Engineering Department Geochemistry Research Laboratory using XRF for principal oxides and ICP-MS for trace elements.

Thin sections of 28 samples were made in Pamukkale University Geological Engineering Department Thin Section Laboratory, and five polished samples were made in Istanbul Technical University Geological Engineering Department Geochemistry Research Laboratory. Thin sections and polishing samples of the study area were examined and photographed by Leica DM2500P polarized microscope at Batman University Geological Engineering Research Laboratory. Microthermometric measurements of fluid inclusions were carried out on 80–120 µm thick doubly polished wafers according to standard

techniques (Roedder 1958, 1972, 1984) at the fluid inclusion laboratory in Istanbul Technical University, using a Linkam THMS G-600 heating–freezing stage. The stage was calibrated with pure H_2O, CO_2, and H_2O-NaCl fluid inclusion standards and potassium dichromate. The accuracy was determined to be ±5°C at high temperatures and ±0.2°C at temperatures below zero. During microthermometry studies, the values of homogenization temperature (Th) and melting temperature (Tm) of the inclusion were measured. Fluid salinities were calculated as wt.% NaCl equivalent using the equation of Bodnar (1993) for the simplified H_2O-NaCl system.

3. Results and discussions

3.1. Geological features of barites

As a result of field observations in the study area, it was determined that two types of barite mineralization offer different features. Both of them are epigenetic vein occurrences,

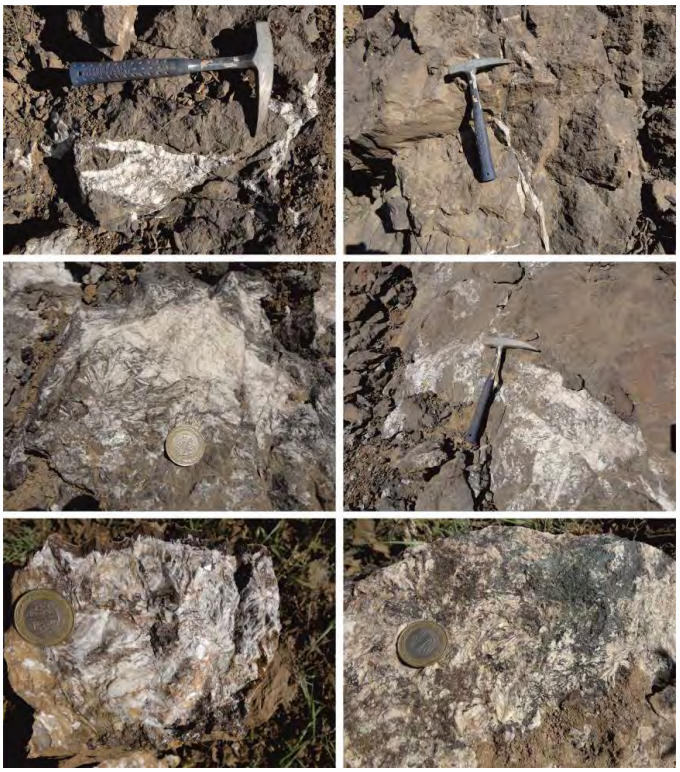

Fig. 4. Field view of first type barites in Meydan formation

Rys. 4. Widok terenowy barytów pierwszego typu w formacji Meydan

with space-filling veins; they occur as massive replacement ores along faults and fractures of host rock. The first of these is observed in the form of thin veins, lenses, mainly radial and large tabular crystals, incompatible with the side rock, in a rich level of iron and manganese oxide in the recrystallized limestones in Meydan formation (Figure 4). These barites are formations in the north of the field and were formed at a lower stratigraphical level than the second type of barites. The main mineral of the veins, whose thickness varies from centimeters to a few 10 centimeters, is barite. Hematite, limonite and malachite (not common) are observed with mineralization (Figure 4).

The second type of barite formation is observed as lenses incompatible with the host rock, that is, recrystallized limestone of Meydan formation, with a thickness ranging from a few centimeters to several decimeters (Figure 5a, b). This barite mineralization contains sulfide minerals such as pyrite, chalcopyrite, bornite, covellite, and chalcocite (Figure 5b, c). Malachite, azurite (rare), iron oxide, and manganese oxides are also observed with barite (Figure 5c, d, e). Alteration zones are observed in the field, along with and around

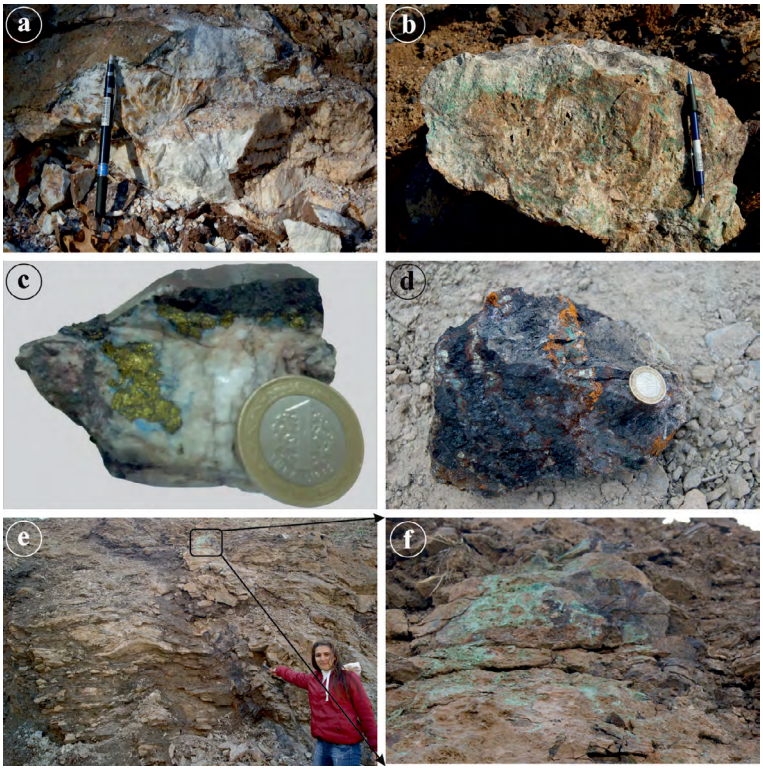

Fig. 5. Field view of second type barites
a – massive barite, b – malachite containing barite, c – barite with chalcopyrite, azurite and iron oxide, d–e – vein rich in sulfide minerals and oxidized minerals, f – malachite

Rys. 5. Widok pola barytów drugiego typu
a – baryt masywny, b – baryt zawierający malachit, c – baryt z chalkopirytem, azurytem i tlenkiem żelaza, d–e – żyła bogata w minerały siarczkowe i minerały utlenione, f – malachit

mineralization, and in different sizes (Figure 6). The most commonly observed alteration in the field consists of hematite-limonite-manganese oxides, and their thickness varies between 1 and 40 centimeters. (Figures 6a, b, c, d). Hematite occurrences (Figure 6e), which develop in the thrust zone and reach several meters in thickness, and limonite occurrences, whose thickness varies from centimeters to 10 centimeters, were also observed (Figure 6f).

Fig. 6. Alterations observed in the study area

Rys. 6. Zmiany zaobserwowane na badanym obszarze

3.2. Ore microscopy

After examining the polished sections belonging to the study area, barite was determined to be the first mineral to be formed. Pyrites are observed in barites, usually in the form of disseminated, subhedral (Figure 7a, c), rarely euhedral crystals (Figure 7b, f). Cataclastic texture, which is observed in pyrite grains, is usually the result of tectonism. These fractures are filled by hematite, goethite, and rarely chalcopyrite (Figure 7c).

Chalcopyrite, which formed after pyrites, surrounded the pyrites, so the pyrites remained in the form of islands within the chalcopyrite (Figure 7b, c, f, g). It has been observed that pyrites were replaced by hematite in different amounts, and hematite acquired a cubic appearance as a result of pseudomorphism due to its almost complete replacement (Figure 7b, c).

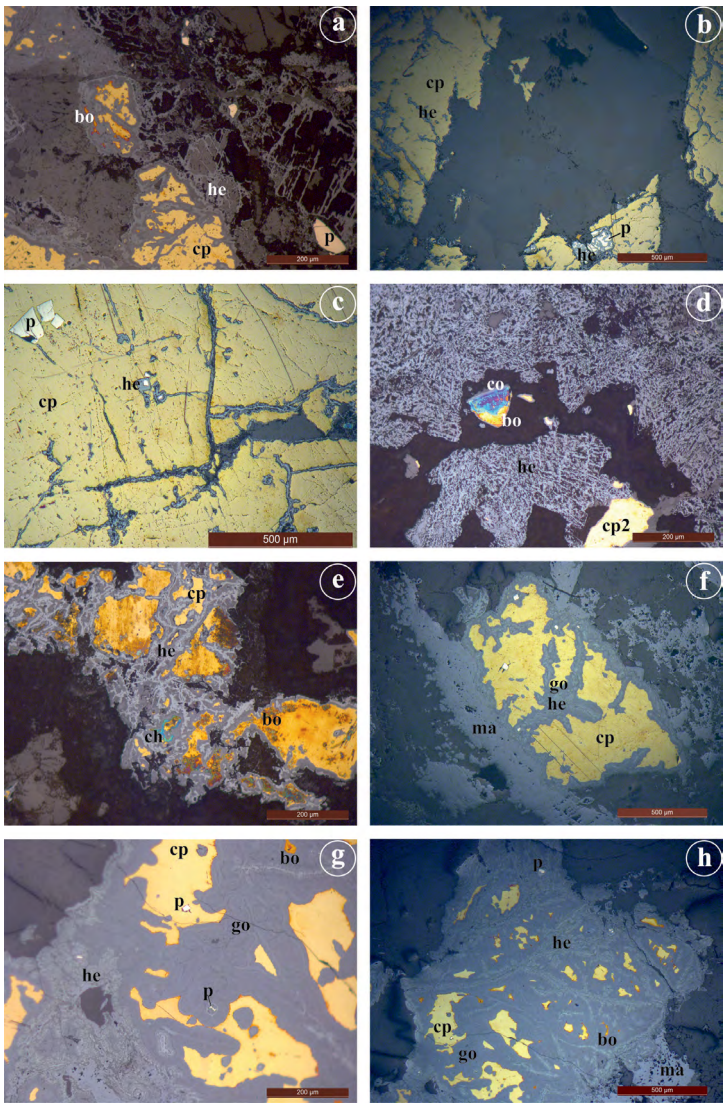

Fig. 7. Microscope images of polished samples
p – pyrite, cp – chalcopyrite, he – hematite, go – goetite, co – covellite, ch – chalcocite, bo – bornite, ma – magnetite

Rys. 7. Obrazy mikroskopowe wypolerowanych próbek
p – piryt, cp – chalkopiryt, on – hematyt, go – goetyt, co – kowelit, ch – chalkozyn, bo – Bornit, ma – magnetyt

As a result of hematite replacing chalcopyrite, hematites were observed to have stockwork texture (Figure 7b, c), boxwork texture (Figure 7e, h), and irregular intrusions (Figure 7a, f, g). Chalcopyrite is irregularly surrounded and replaced by goethite and hematite along its border (Figure 7a, f, g). It has been determined that goethite and hematite have irregular inclusions (Figure 7f) and colloform structures (Figure 7g).

Hematite formations presenting boxwork and stockwork texture in the fractures and cavities of barites are an indicator of hydrothermal formation. The enrichment minerals bornite substituted chalcopyrites, covellite (less), and chalcocite (less) (Figure 7a, d, e, g, h). Magnetites were formed after the goethite, and it was observed that they surrounded them. (Figure 7f, h). Since iron-oxide minerals are abundantly observed in the samples, boxwork, coliform textures, and trellis structure characteristics for these minerals are frequently observed (Figure 7a, d, e, g, h). As a result of examining the samples, two separate chalcopyrite formations were determined. The first chalcopyrite (cp) was replaced by bornite, covellite, and chalcocite in different amounts. Second, chalcopyrite (cp2) is not replaced because it is formed later stage (Figure 7d, g). As a result of microscopic studies, the mineral assemblage of mineralization is barite ± chalcopyrite ± hematite ± goethite ± magnetite ± bornite ± ± chalcocite ± covellite ± malachite ± limonite ± manganese oxide (Figure 8).

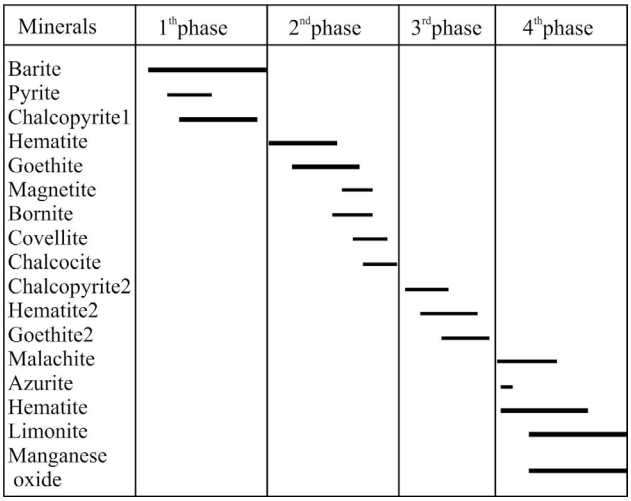

Fig. 8. Paragenetic sequence of study area

Rys. 8. Sekwencja paragenetyczna obszaru badań

3.3. Fluid inclusion study

Within the scope of fluid inclusion studies conducted on barite samples, primary and total fluid inclusions were determined, homogenization temperature (Th) and melting

temperature (Tmice) values were measured from the primary inclusions, and salinity values of the inclusions were calculated according to Bodnar (1993) (Figure 9). It was determined that the inclusions had sizes varying between 50.1–191 μm; all of them were simple two-phase inclusions dominated by the liquid phase, and the gas phase consisted of water (Figure 10).

As a result of the evaluation of fluid inclusion measurements, it was seen that the barites formed stratigraphically lower in the Meydan formation, at a level rich in iron and manganese oxides, had high salinity and temperature values. It has been determined that barites observed at stratigraphically up levels within the formation have low salinity and temperature values. This grouping observed as a result of the distribution of values shows that the solution causing barite formation has multiple origins. The first of these is seawater

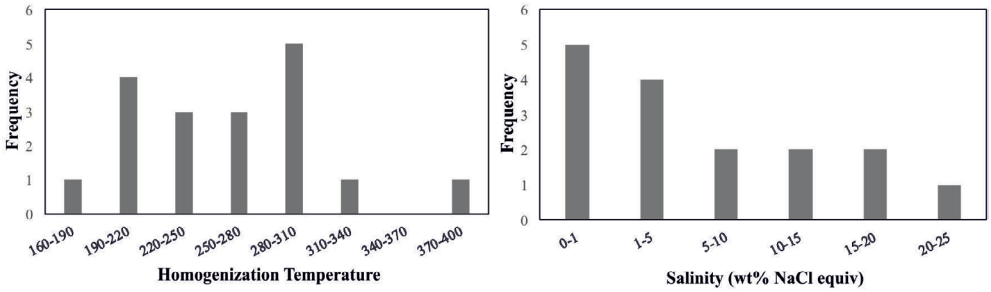

Fig. 9. Frequency histogram of fluid inclusion parameters of Sason barites

Rys. 9. Histogram częstotliwości parametrów inkluzji płynnych barytów Sasona

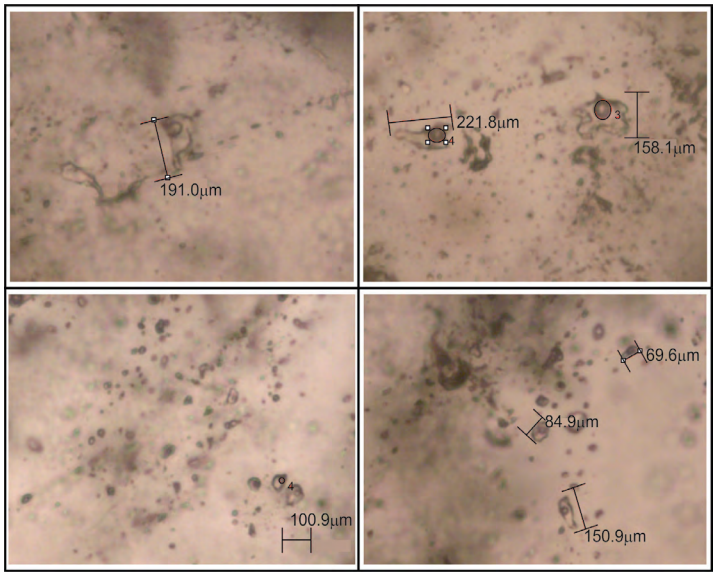

Fig. 10. Fluid inclusions observed in barite minerals

Rys. 10. Wtrącenia płynne obserwowane w minerałach barytu

that is heated by hydrothermal cycling through discontinuities in the sea floor and whose salinity value increases with the elements it absorbs by leaching from the rocks it passes through. The other is a diluted solution mixture resulting from the addition of meteoric waters with lower temperature and salinity values as mineralization from seawater continues (Figure 11).

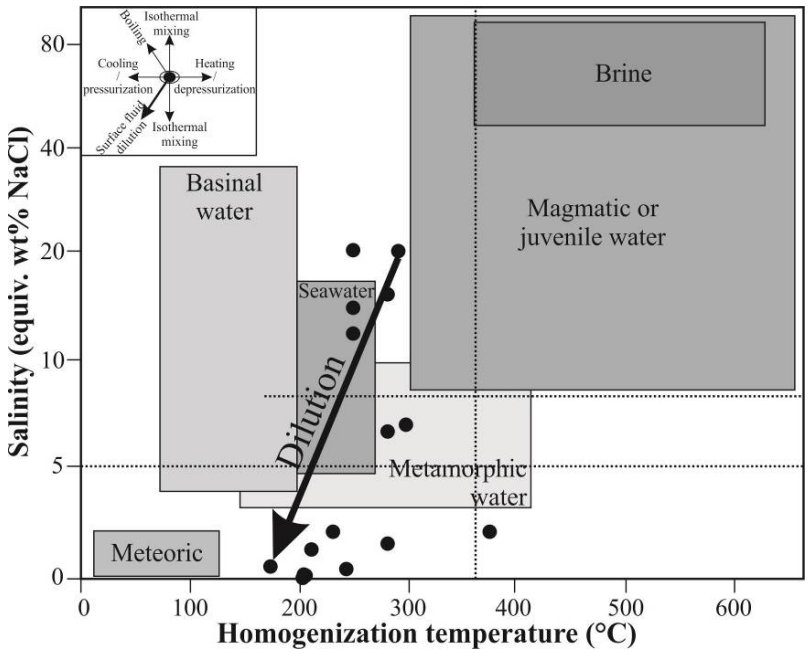

Fig. 11. Determination of the origin of the solution that caused its formation by using the liquid inclusion values of barites (Wilkinson 2001 (schematic diagram at top left showing typical trends); Kesler 2005)

Rys. 11. Określenie pochodzenia roztworu, który spowodował jego powstanie, na podstawie wartości wtrąceń ciekłych barytów

Observation of the salinity values of fluid inclusions in a wide range ranging from high salinity to low salinity is interpreted as dilution as a result of the mixing of meteoric waters (Wilkinson 2001; Asl et al. 2015).

3.4. Geochemistry

25 samples taken from the units observed in the study area were analyzed by the main oxides XRF and trace and rare earth elements ICP-MS in Istanbul Technical University, Faculty of Mining, Geological Engineering Department, Geochemistry Research Laboratory (Table 1, 2).

Table 1. Main oxide and some trace element contents of the samples (anoxides wt%, trace elements in ppm)

Tabela 1. Zawartość głównych tlenków i niektórych pierwiastków śladowych w próbkach (% wag. beztlenków, pierwiastki śladowe w ppm)

	SiO_2	TiO_2	Al_2O_3	Fe_2O_3	MnO	MgO	CaO	Na_2O	K_2O	BaO	LOI	SUM	Cu	Pb	Zn
1B	2.16	0.02	0.70	0.48	0.16	0.80	51.91	ND	0.29		43.45	100	9	8	11
2B	36.83	0.31	7.93	4.08	0.26	3.59	22.17	0.03	2.38		22.19	99.93	17	7	29
3	42.13	0.03	0.76	11.97	1.06	5.21	18.25	0.02	0.23		19.93	99.86	12	26	0.15
5	2.22	0.01	0.08	64.52	4.28	3.85	6.59	ND	0.02		16.36	99.16	848	12	328
8	5.32	0.02	0.37	1.43	0.18	1.79	57.1	ND	0.14		33.55	99.92	10	3	18
10	25.8	0.01	0.28	36.19	3.43	3.89	6.41	ND	0.06		23.21	99.4	0.1		34
11	25.16	0.05	1.42	1.48	0.16	0.56	42.8	ND	0.50		27.83	100	11	13	15
13A	15.89	0.08	1.34	11.27	1.27	11.54	23.39	ND	0.31		34.57	99.88	700	15	75
14BA	0.89	0.003	0.10	4.00	0.36	17.88	31.02	ND	0.02		45.47	99.95	11	8	26
20	22.52	0.43	4.52	2.99	0.06	4.25	34.38	0.44	0.79		29.12	99.87	19	29	65
21	15.82	0.22	3.67	2.76	0.13	2.27	39.41	0.25	0.86		34.18	99.9	23	14	41
23A	92.37	0.01	0.18	2.66	0.004	0.05	2.11	ND	0.03		2.50	99.92	35	8	4
24	10.28	0.01	0.27	43.29	2.29	4.54	8.46	ND	0.05	1.27	27.98	99.27	0.16	35	98
25A	7.47	0.01	0.08	23.12	2.01	6.08	20.23	ND	0.01		34.57	99.56	174	2	29
29A	60.47	0.69	13.79	5.67	0.09	6.21	3.78	3.50	1.54		3.87	99.86	37	16	46
30	24.85	0.32	5.95	3.80	0.24	1.85	33.79	1.46	0.81		26.63	99.89	35	12	53
31B	13.88	0.10	1.65	1.97	0.07	6.23	40.15	0.31	0.32		35.05	99.84	11	9	24
32_Dere	19.55	0.08	3.49	2.88	0.1	14.66	25.76	0.06	0.87		31.87	99.75	6	8	30
35	9.32	0.15	2.80	1.13	0.01	0.67	48.60	0.29	0.55		35.92	99.85	29	21	13
14A	4.23	0.04	0.09	43.36	3.3	1.93	1.38	0.22	ND	25.25	6.99	99.85	0.09	4	116
18	34.94	2.61	13.34	15.10	0.28	5.59	12.26	2.24	0.96		11.69	99.7	79	9	127
25C2	12.97	0.04	0.92	51.07	2.17	0.64	1.33	ND	0.21		12.55	99.81		117	
27BM	86.16	0.46	3.20	3.47	0.18	0.24	0.69	0.04	0.77		2.91	99.59	8,400	90	10
27	1.83	0.11	ND	0.26	0.02	ND	0.02	0.65	ND	61.60	2.38	99.99	28,964	6,752	1,111
27A	1.97	0.15	ND	0.32	0.05	ND	0.35	0.45	ND	60.00	2.42	99.99	244		49

Table 2. Rare earth element contents of the samples

Tabela 2. Zawartość pierwiastków ziem rzadkich w próbkach

	La	Ce	Pr	Nd	Sm	Eu	Gd	Tb	Dy	Ho	Er	Tm	Yb	Lu	Th
1B	10.53	8.46	2.20	9.19	2.08	0.53	2.78	0.42	2.58	0.57	1.64	0.23	1.39	0.23	1.32
2B	23.55	32.82	5.96	23.18	4.59	0.92	4.96	0.69	3.98	0.76	2.10	0.28	1.71	0.25	5.07
3	9.15	11.50	1.88	7.37	1.57	1.11	1.87	0.27	1.54	0.31	0.88	0.13	0.81	0.13	0.78
5	17.53	31.97	4.42	17.45	7.07	5.91	3.56	0.46	2.34	0.42	1.04	0.15	0.73	0.46	0.10
8	5.55	5.17	1.12	4.50	0.96	0.33	1.17	0.17	0.96	0.19	0.54	0.07	0.46	0.10	0.35
10	6.81	9.76	1.53	5.88	1.16	0.98	1.37	0.19	1.10	0.22	0.60	0.07	0.42	0.06	0.42
11	11.35	9.90	2.67	11.06	2.40	0.60	2.89	0.42	2.38	0.49	1.31	0.17	0.97	0.14	1.34
13A	12.11	13.22	2.04	8.11	1.81	0.89	2.09	0.29	1.66	0.33	0.88	0.12	0.67	0.11	0.79
14BA	2.81	2.79	0.65	2.78	0.71	0.31	0.93	0.14	0.86	0.19	0.56	0.08	0.47	0.09	0.15
20	14.39	28.58	4.00	16.32	3.50	0.86	3.41	0.48	2.60	0.48	1.29	0.18	1.09	0.17	2.87
21	12.87	15.61	2.68	10.16	2.14	0.56	2.22	0.32	1.81	0.37	1.08	0.16	0.97	0.17	2.29
23A	0.41	0.92	0.13	0.52	0.15	0.05	0.23	0.04	0.30	0.08	0.39	0.04	0.38	0.06	0.19
24	6.78	12.55	1.83	7.50	4.80	3.35	1.95	0.30	1.77	0.34	0.93	0.15	0.78	0.40	0.33
25A	9.06	19.65	2.70	11.19	3.05	1.67	3.69	0.45	2.07	0.33	0.74	0.08	0.39	0.06	0.11
29A	13.93	24.72	3.35	13.46	3.08	1.03	3.28	0.49	2.82	0.59	1.67	0.24	1.52	0.24	3.89
30	13.22	18.68	3.19	13.03	2.96	0.91	3.10	0.45	2.62	0.53	1.54	0.22	1.41	0.24	2.42
31B	7.60	15.29	1.99	7.98	1.75	0.54	1.75	0.25	1.43	0.28	0.76	0.10	0.60	0.09	1.63
32_Dere	10.65	22.87	3.03	12.61	2.96	0.59	3.20	0.50	2.87	0.54	1.46	0.19	1.10	0.16	1.66
35	13.69	29.71	3.68	14.05	2.58	0.57	2.65	0.38	2.11	0.39	1.00	0.13	0.66	0.13	2.22
14A	5.90	9.60	1.30	4.94	12.20	8.62	1.04	0.13	0.60	0.11	0.25	0.14	0.63	1.10	0.04
18	25.80	52.41	7.85	34.63	7.55	2.60	8.68	1.28	7.20	1.33	3.45	0.44	2.51	0.31	2.82
25C2	7.27	14.95	2.05	8.13	1.88	1.54	1.94	0.27	1.42	0.26	0.64	0.07	0.41	0.06	0.67
27BM	10.38	13.32	1.33	4.62	1.73	0.97	1.43	0.23	1.46	0.30	0.85	0.14	1.00	0.20	2.36
27	8.62	13.08	1.53	5.57	14.75	10.56	1.23	0.17	0.89	0.16	0.40	0.15	0.75	1.11	0.35
27A	0.62	0.39	0.04	0.14	6.15	4.16	0.02	0.00	0.01	0.00	0.00	0.06	0.27	0.58	0.01

Rare Earth Elements (REE) Geochemistry.

Barites are generally rich in Fe_2O_3 (0.26–51.07 wt%) and SiO_2 (1.83–34.94 wt%) (except for a silicified sample with 86.16 wt% content), while BaO contents range from 25.25––61.6 wt%, Al_2O_3 (0.09–13.34 wt%), TiO_2 (0.04–2.61 wt%), MnO (0.02–3.3 wt%), MgO (0.24–5.59 wt%), CaO (0.02–12.26 wt%). Barites high SrO (2.04–3.64 wt%) content is indicative of hydrothermal origin (Werner 1958; Starke 1969). These values are similar to those in Türkiye and in the world known as barite vein-type beds, and they are even higher than they are (Tas Ozdogan et al. 2017). The main oxide content of the host rocks is SiO_2 (0.89–60.47 wt%), Al_2O_3 (0.08–13.79 wt%), Fe_2O_3 (0.48–64.52 wt%), MnO (0.004––4.28 wt%), MgO (0.05–17.88 wt%), CaO (2.11–51.91 wt%) (Table 1).

Although barites have low trace element content, only sample 27 contains high Cu (28,964 ppm), Pb (6,752 ppm), Zn (1,111 ppm), and Sr (1,363 ppm) (Table 1). High Sr content of barites is indicative of low-temperature hydrothermal formation. The change of SiO_2 content of barites and side rocks som,e of them offering high values, are also indicators of silicification.

The rare earth element geochemistry of samples taken from Kizilagac, Tutu, and Meydan formations observed in the region provides results that are consistent with the origin. Since the Tutu Formation is a volcanic rock formed in a marine environment, it indicates chondrite in terms of heavy rare earth elements (HREE). Negative Ce and Eu peaks indicate a marine environment (Figure 12a). Kizilagac formation reflects the typical terrestrial environment effect with its high rare earth element content, being rich in LREE and positive Eu peak (Figure 12b). Since the Maden formation, which is a host rock to barites (barites are sometimes observed along the border with Kizilagac formation), was formed on the passive continental edge, it is geologically normal for there to be terrestrial interaction. The samples of the Meydan formation have a high rare earth element content, are rich in LREE, have a typical continental crust pattern, and have a positive Eu peak, indicating that they are affected by a terrestrial hydrothermal system. It has been observed that while the ∑REE and LREE contents of the stratigraphically lower and barite-free levels of the unit are low, the ∑REE and LREE contents are very high in the upper and barite-containing levels. Although the REE patterns of host rocks and barite are almost the same, the Eu values of barite are higher (Figures 12c, 13b).

Since Light Rare Earth Element (LREE) patterns are different in different marine environments, they assist in determining the storage environments of barites (Guichard et al. 1979; DeBarr et al. 1985). While negative Ce and Eu values are characteristic of seawater, the positive anomaly is characteristic of Eu values in hydrothermal solutions (Guichard et al. 1979; Baar et al. 1985; Elderfield 1988).

Taylor and Mclennan (1985) used the chondrite value of the samples in the study area to normalize them. While drawing REE patterns, known hydrothermal formations such as Salton Sea (Michard 1989) and EPR21 (Michard and Albarede 1986) were compared with Hasköy barites that are similar in terms of geological environment and formation to the region with seawater. Kumral (2010) stated that the seawater and hydrothermal fluids are effective in the formation of Hasköy barites, suggesting that the negative Ce peak characterizes the seawater and that the positive Eu is an indicator of hydrothermal interaction. As can be

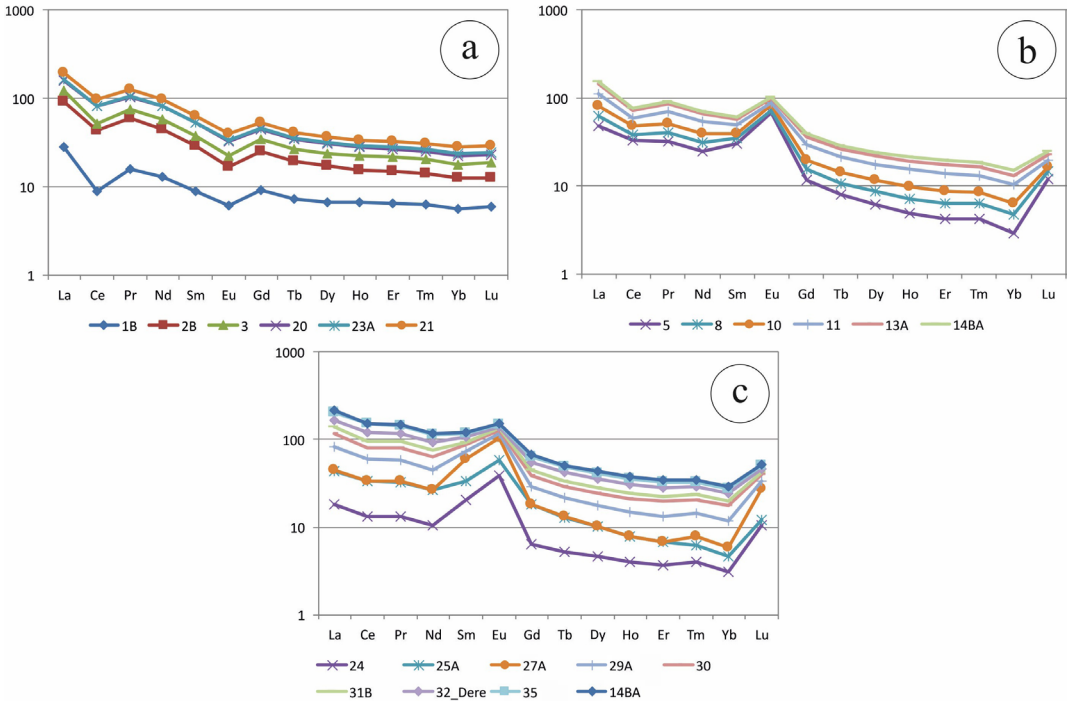

Fig. 12. REE normalized diagrams of different formations and barites in the study area
a – Tutu formation, b – Kizilagac formation, c – Meydan formation

Rys. 12. Znormalizowane diagramy REE różnych formacji i barytów na badanym obszarze
a – formacja Tutu, b – formacja Kizilagac, c – formacja Meydan

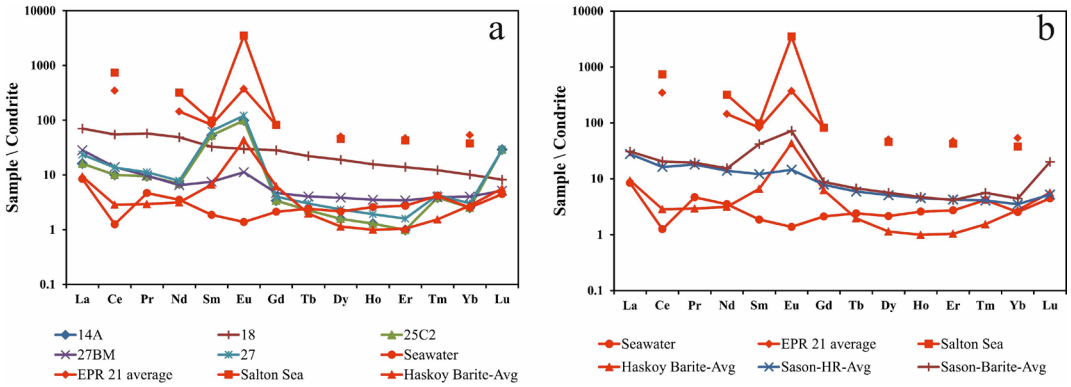

Fig. 13. Rare Earth Element patterns of samples
a – comparison of REE patterns of barite samples,
b – comparison of average REE patterns of barites and side rocks, HR – host rock, Avg – average

Rys. 13. Wzory próbek pierwiastków ziem rzadkich
a – porównanie rozkładu REE próbek barytu,
b – porównanie średnich rozkładów REE barytów i skał bocznych, HR – skała macierzysta, Avg – średnia

seen from the REE patterns of the Salton Sea and EPR21, the highly positive Eu value is a characteristic of hydrothermal systems. The negative Ce peak (not very obvious) observed in the rare earth element patterns of the barite samples shows that seawater affects their formation. In contrast, the positive Eu peak reflects the effect of the hydrothermal fluids (Figure 13a, b).

In addition, when the rare earth element pattern of the samples is correlated with the average seawater pattern, which plays an important role in the formation of the host rock, it is seen that the amount of rare earth elements is wealthy and different (Figure 13a, b). When the REE averages of host rocks and barites were compared with the same environments, it was determined that the REE patterns of barites and host rocks were almost the same but differed only in terms of Sm, Eu, and Lu.

Eu/Eu* values of barites vary between 11.20–121.36, indicating exhalative hydrothermal fluids of barites (Barret et al. 1990). The elements Eu and Ba are very similar in diameter and electric value. Eu/Eu* > 1 (positive anomaly, Taylor and McLennan 1981) in barites are associated with metamorphic sedimentary processes. Positive Eu anomaly may indicate the mixture of two fluids, high oxygen fugacity, and oxidized ore formation for barites. Ce/La > 1 (10.03–54.76) indicates terrestrial origin for barites (Guichard et al. 1979). Negative Ce/Ce* ratios of the samples indicate the oxidation state of the seawater environment (Bhattacharya et al. 2007). Since the Ce/Ce* values of the samples are less than 0.5, they indicate open seawater and related deposits (Elderfield 1988; Ehya 2012).

The fact that barites in the study area have LaN/YbN > 1 indicates that the LREE concentration is high. The high concentrations of LREE indicate they can act as the preparation of carrier complexes in parental fluids. The ratio of CeN/YbN of the samples is >1, which indicates that LREE values are highly concentrated compared to HREE values. The TbN/LaN ratio shows the change in the deposition environment. While LREE is enriched in primary formations, HREE enrichment is observed in late formations (Palinkas et al. 1994). This indicates a change in the storage environment. Since the ratio of TbN/LaN is <1 in all samples, it indicates HREE enrichment in the samples. The LaN/SmN being > 1 causes LREE to be observed at higher concentrations compared to HREE and high concentrations of Ce and Tm to be observed in the hydrothermal fluid. While this ratio is LaN/SmN > 1 in samples at a stratigraphically lower level, it is LaN/SmN <1 in samples at a higher level (Hajalilou et al. 2014).

Sediments precipitated from hydrothermally influenced seawater have distinctive features, including an LREE-enriched pattern, low Ce anomaly, and low Ce/La ratios (Guichard et al. 1979; Alexander et al. 2008).

As can be seen from the normalized Ce-Sm and Ce-Yb diagram of the study samples (Figure 14), barites and side rocks offer values that change from seawater to the terrestrial hydrothermal system. While the side rocks appear closer to the sea water, the barites show similarity to the terrestrial samples, while pointing to the marine origin of the side rocks is an indication of the barites affected by the terrestrial environment. These data confirm the observations made by field observations and REE.

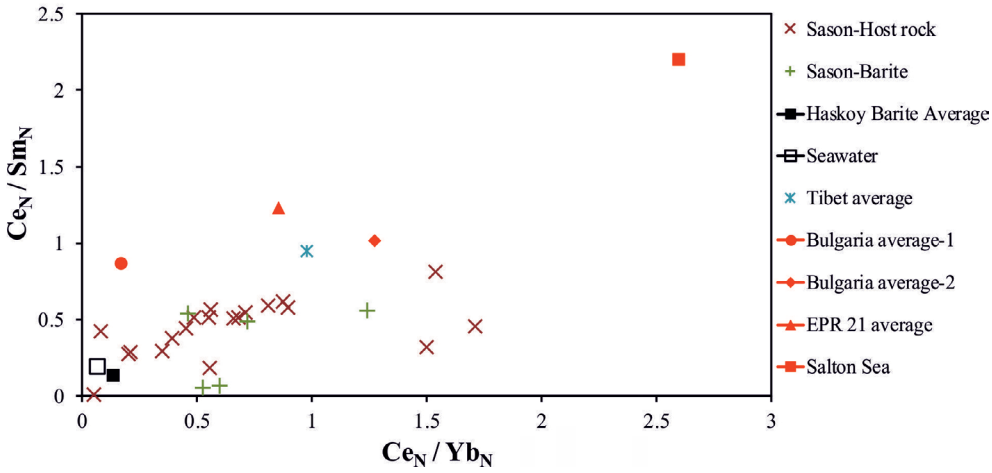

Fig. 14. Ce_N/Sm_N – Ce_N/Yb_N diagram of the samples

Rys. 14. Wykres Ce_N/Sm_N – Ce_N/Yb_N próbek

Due to the difference in mineral paragenesis, barites (first and second type barites), which are divided into two types, are actually formations observed in the same host rock and have similar formation types. The main reason for the difference in paragenesis, Eu content, and fluid inclusion values of the two barites is the mixing and interaction amounts of sea water and terrestrial hydrothermal fluids that caused their formation.

Conclusions

The units observed in the study area cover a wide age range, crossing the Paleozoic, Mesozoic, and Cenozoic eras, and their shared boundaries are generally observed to have tectonic contact. Since the study area is located just north of the Bitlis–Zagros suture belt, it was exposed to intense tectonism during the closure of the Tethys Ocean. As a result, there are many tectonic structures in the area and environments in which hydrothermal solutions can easily move.

The mineralization observed in the study area is irregular in shape, such as veins and lenses within the Devonian Meydan formation. The main mineral is barite, accompanied by iron and manganese oxides and sulfur minerals. The mineralization consists of barite ± ± chalcopyrite ± hematite ± goethite ± magnetite ± bornite ± chalcocite ± covellite ± ± malachite ± limonite ± manganese oxide.

The formations of hematite, limonite, and malachite (less frequently) observed in the study area indicate the presence of an intense hydrothermal alteration. These minerals are an indication that the hydrothermal system that caused the alterations also caused mineralization

as they are closely related to the ore minerals, as determined by field observations and microscope studies. This indicates that the mineralization developed after the host rock.

The fact that the fluid inclusion results of barites show a trend from high temperature and salinity to low temperature and salinity shows that dilution occurred as a result of a hydrothermal interaction with the primary solution that provided the formation of barites.

The $BaSO_4$ content of the barite samples varies between 25.25 wt% and 61.6 wt%, and the high SrO content is an indication of hydrothermal origin. The average REE content of the barites and host rocks are similar to each other, while the barites show a strongly positive Eu peak, indicating a terrestrial interaction. The distribution of sample values in the Ce_N/Sm_N – Ce_N/Yb_N diagram indicates the transition from seawater to terrestrial hydrothermal systems.

Eu/Eu* values of barites indicate exhalative hydrothermal fluids of barites, Ce/La values indicate terrestrial origin, Ce/Ce* values of the samples indicate open seawater and related deposits. While the La_N/Yb_N, Ce_N/Yb_N, and Tb_N/La_N ratios of the samples indicate LREE enrichment, the Tb_N/La_N and La_N/Sm_N ratios indicate HREE enrichment. As a result of:

1. The irregular shape of the mineralization its incompatible with the host rock, ore microscopy studies.
2. Liquid inclusion values indicate a dilution from high temperature and salinity to low temperature and salinity
3. REE content of barites is similar to its host rocks.
4. The Eu/Eu* ratio indicates exhalative hydrothermal origin, the Ce/La ratio indicates the terrestrial environment, and the Ce/Ce* ratio indicates seawater and related deposits.

It shows that barites are formed from hydrothermally affected sea water.

The Author have no conflict of interest to declare.

REFERENCES

Akıncı, Ö.T. 2009. Ophiolite-hosted Copper and Gold Deposits of Southeastern Turkey: Formation and Relationship with Seafloor Hydrothermal Processes. *Turkish Journal of Earth Sciences* 18, pp. 475–509, DOI: 10.3906/yer-0803-8.

Akkoca, D.B. and Çelebi, H. 2018. The Massive Sulfide Deposit of Siirt Madenköy, South-Eastern Turkey. *Journal of Minerals and Materials Characterization and Engineering* 6, pp. 155–178, DOI: 10.4236/jmmce.2018.62012.

Alaminia, Z. and Sharifi, M. 2018. Geological, geochemical and fluid inclusion studies on the evolution of barite mineralization in the Badroud area of Iran. *Ore Geology Reviews* 92, pp. 613–626, DOI: 10.1016/j.oregeorev.2017.12.011.

Asl et al. – Asl, S.M., Jafari, M., Sahamiyeh, R.Z. and Shahrokhi, V. 2015. Geology, geochemistry, sulfur isotope composition, and fluid inclusion data of Farsesh barite deposit, Lorestan Province, Iran. *Arabian Journal of Geosciences* 8, pp. 7125–7139, DOI: 10.1007/s12517-014-1673-7.

Babaei, A.H. and Ganji, A. 2018. Characteristics of the Ahmadabad hematite/barite deposit, Iran – studies of mineralogy, geochemistry and fluid inclusions. *Geologos* 24(1), pp. 55–68, DOI: 10.2478/logos-2018-0004.

Barrett et al. 1990 – Barrett, T.J., Jarvis, I. and Jarvis, K.E. 1990. Rare earth element geochemistry of massive sulfides-sulfates and gossans on the Southern Explorer Ridge. *Geology* 18, pp. 583–586, DOI: 10.1130/0091-7613(1990)018%3C0583:REEGOM%3E2.3.CO;2.

Bhattacharya et al. 2007 – Bhattacharya, H.N., Chakraborty, I. and Ghosh, K. 2007. Geochemistry of some banded iron formations of the Archean supracrustal, Jharkhand-Orissa region, India. *Journal of Earth System Science* 116(3), pp. 245-259, DOI: 10.1007/s12040-007-0024-4.

Bodnar, R. 1993. Revised equation and table for determining the freezing point depression of H_2O-NaCl solutions. *Geochimica et Cosmochimica Acta* 57, pp. 683–684, DOI: 10.1016/0016-7037(93)90378-A.

Boray, A. 1973. The structure and metamorphism of the Bitlis area, Turkey. Ph. D. Thesis, University of London, London, England.

Çiftçi, E. 2019. Volcanogenic Massive Sulfide (VMS) Deposits of Turkey. [In:] Pirajno F. et al. eds. Mineral Resources of Turkey. *Modern Approaches in Solid Earth Sciences*, vol 16. Switzerland: Springer, pp 427–495, DOI: 10.1007/978-3-030-02950-0_9.

DeBarr et al. 1985 – DeBarr, H.J.W., Bacon, M.P. Brewer, P.G. and Bruland, K.W. 1985. Rare earth elements in the Pacific and Atlantic Oceans. *Geochimica et Cosmochimica Acta* 49, pp.1943–1959, DOI: 10.1016/0016-7037(85)90089-4.

Derakhshi et al. – Derakhshi, M.G., Hosseinzadeh, M.R., Moayyed, M. and Maghfouri, S. 2020. Geological, isotope geochemical and fluid inclusion constraints on the Mishu SEDEX-type Barite (Pb-Cu-Zn) system, NW Iran. *Ore Geology Reviews* 121, DOI: 10.1016/j.oregeorev.2020.103493.

Ehya, F. 2012. Rare earth element and stable isotope (O, S) geochemistry of barite from the Bijgan deposit, Markazi Province, Iran. *Mineralogy and Petrology* 104, pp. 81–93, DOI: 10.1007/s00710-011-0172-8.

Ehya, F. and Mazraei, S.M. 2017. Hydrothermal barite mineralization at Chenarvardeh deposit, Markazi Province, Iran: Evidences from REE geochemistry and fluid inclusions. *Journal of African Earth Sciences* 134, pp. 299––307, DOI: 10.1016/j.jafrearsci.2016.11.006.

Elderfield, H. Whitfield, M. Burton, J.D. Bacon, M. P. and Liss, P.S. 1988. The Oceanic Chemistry of the Rare-Earth Elements. *Philosophical Transactions of the Royal Society of London. Series A, Mathematical and Physical Sciences* 325, no. 1583, pp. 105–126. [Online:] http://www.jstor.org/stable/38104.

Ghorbani, M. 2013. *The Economic Geology of Iran, Mineral Deposits and Natural Resources*. Springer Geology, Dordrecht, 572 pp., DOI: 10.1007/978-94-007-5625-0.

Göncüoğlu, M.C. and Turhan, N. 1985. Bitlis Metamorfik Kuşağının Orta Bölümünün Temel Jeolojisi, Maden Tetkik ve Arama Müdürlüğü (MTA), *MTA Raporu Derleme no 7707*, Ankara, Türkiye (*in Turkish*).

Guichard et al. – Guichard, F. Church, T.M. Treuil, M. and Jaffrezic, H. 1979. Rare earths in barites: distribution and effects on a queous partitioning. *Geochimica et Cosmochimica Acta* 43, pp. 983–997, DOI: 10.1016/0016-7037(79)90088-7.

Hajalilou et al. 2014 – Hajalilou, B. Vusuq, B. and Moayed, M. 2014. REE Geochemistry of Precambrian Shale-Hosted Barite-Galena Mineralization, a Case Study from NW Iran. *Journal of Crystallography and Mineralogy* 22(2), pp. 39–48.

Hanilçi et al. 2016 – Hanilçi, N. Öztürk, H. Banks, D.A. and Koral, H. 2016. Carbonate-Hosted Zn-Pb deposits in the Hakkari-Şırnak region: a newly discovered Tethyan Metallogenic province in Turkey. *SEG 2016 conference*, Çeşme, Turkey, September, pp. 25–28.

Hanilçi et al. 2017 – Hanilçi, N. Öztürk, H. and Banks, D.A. 2017. Geochemical stratigraphy of the Karakaya non-sulphide Zn-Pb deposit, Hakkari, SE Turkey, *Proceedings of the 14th SGA Biennial Meeting*, Canada, August, pp. 669–671.

Hanilçi et al. 2018 – Hanilçi, N. Öztürk, H. and Banks, D.A. 2018. Trace element and stable sulpur isotope geochemistry of the Hakkari region Zn-Pb deposits. *8th Geochemistry symposium*, Antalya, Turkey, May, pp. 194–195.

Hanilçi et al. 2019 – Hanilçi, N. Öztürk, H. and Kasapçi, C. 2019. Carbonate-Hosted Pb-Zn Deposits of Turkey. [In:] Pirajno F., Ünlü T., Dönmez C., and Şahin M. (eds). *Mineral Resources of Turkey. Modern Approaches in Solid Earth Sciences* 16, pp. 497–534, DOI: 10.1007/978-3-030-02950-0_10.

Hormozi et al. 2023 – Hormozi, H.K., Ehya, F. Paydar, P.R. and Kheymehsari, S.M. 2023. Formation of barite in the Ab Torsh deposit, Kerman province, Iran: Insights from rare earth elements, O and S isotopes, and fluid inclusions. *Geochemistry* 83(4), DOI: 10.1016/j.chemer.2023.126024.

Kato, Y. 1999. Rare earth elements as an indicator to origins of skarn deposits: Examples of the Kamioka Zn-Pb and Yoshiwara-Sannotake Cu(-Fe) deposits in Japan. *Resource Geology* 49, pp. 183–198, DOI: 10.1111/j.1751-3928.1999.tb00045.x.

Kesler, S.E. 2005. Ore-forming fuids. *Elements* 1(1), pp. 13–18, DOI: 10.2113/gselements.1.1.13.

Kumral, M. 2010. Mineralogical, geochemical, and isotopic (Sr, O, S) evidence for multiple fluid sources for the Hasköy barite deposits, SE Anatolia, Turkey. *Fresenius Environmental Bulletin* 19(2), pp. 208–220.

Okay, A.I. 2008. Geology of Turkey: A synopsis. *Anschnitt* 21, pp. 19–42.

Palinkas L.A. and Jurkovic I. 1994. Lanthanide geochemistry and fluid inclusion peculiarities of the fluorite form the barite deposits south of Kresevo (Bosnia and Herzegovina). *Geologia Croatia* 47(1), pp. 103–115.

Roedder, E. 1958. Technique for the extraction and partial chemical analysis of fluid-filled inclusions from minerals. *Economic Geology* 53, pp. 235–269, DOI: 10.2113/gsecongeo.53.3.235.

Roedder, E. 1972. *Compostion of Fluid Inclusion*. U.S. Geological Survey: Reston, VA, USA.

Roedder, E. 1984. *Fluid Inclusions*. Mineralogical Society of America: Chantilly, VA, USA, DOI: 10.1515/9781501508271.

Santoro et al. 2013 – Santoro, L. Boni, M. Herrington, R. and Cleeg, A. 2013. The Hakkari nonsulfide Zn-Pb deposit in the context of other nonsulfide Zn-Pb deposits in the Tethyan Metallogenic Belt of Turkey. *Ore Geology Reviews* 53, pp. 244–260, DOI: 10.1016/j.oregeorev.2013.01.011.

Şaşmaz et al. 2014 – Şaşmaz, A. Türkyilmaz, B. Öztürk, N. Yavuz, F. and Kumral, M. 2014. Geology and geochemistry of Middle Eocene Maden complex ferromanganese deposits from the Elazığ–Malatya region, eastern Turkey. *Ore Geology Reviews* 56, pp. 352–372, DOI: 10.1016/j.oregeorev.2013.06.012.

Starke, R. 1969. *Die Strontiumgehalte der Baryte*. *Freiberger Forschungsh* 150, pp. 86 (*in German*).

Tas Ozdogan et al. 2017 – Tas Ozdogan, A. Uras, Y. and Oner, F. 2017. Geochemistry of the barite deposits near Adana-Feke area (Eastern Taurides). *Russian Geology and Geophysics* 58, pp. 1351–1367, DOI: 10.1016/j.rgg.2017.11.003

Taylor S.R. and McLennan S.M. 1981. The composition and evolution of the continental crust: rare earth element evidences from sedimentary rocks. *Philosophical Transactions of the Royal Society of London. Series A, Mathematical and Physical Sciences* 301, pp. 381–399, DOI: 10.1098/rsta.1981.0119.

Taylor, S.R. and McLennan, S.M. 1985. *The Continental Crust; Its composition and evolution; an examination of the geochemical record preserved in sedimentary rocks*. Oxford, Blackwell, pp. 312. [Online:] https://api.semanticscholar.org/CorpusID:126912766.

Werner, C.D. 1958. *Geochemie und paragenese der saxonischen schwerspat–flusspat–gaenge im schmalkaldener revier*. Freiberger Forschungshf, Berlin. pp. 47 (*in German*).

Wilkinson, J.J. 2001. Fluid inclusions in hydrothermal ore deposits. *Lithos* 55, pp. 229–272, DOI: 10.1016/S0024-4937(00)00047-5.

Yılmaz et al. 1987 – Yılmaz, Y. Şaroğlu, F. and Güner, Y. 1987. Initiation of the neomagmatism in East Anatolia. *Tectonophysics* 134, pp. 177–199, DOI: 10.1016/0040-1951(87)90256-3.

Yılmaz et al. 1993 – Yılmaz, Y. Yiğitbaş, E. and Denç, C.Ş. 1993. Ophiolitic and metamorphic assembleges of southeast Anatolia and their significance in the geological evolution of the orogenic belt. *Tectonics* 12(5), pp. 1280–1297, DOI: 10.1029/93TC00597.

Zarasvandi et al. 2014 – Zarasvandi, A., Zaheri, N., Pourkaseb, H., Chrachi, A. and Bagheri, H. 2014. Geochemistry and fuid-inclusion micro thermometry of the Farsesh barite deposit, Iran. *Geologos* 20(3), pp. 201–214, DOI: 10.2478/logos-2014-0015.

GEOCHEMISTRY AND FLUID-INCLUSION MICROTHERMOMETRY OF THE ORENAGIL BARITE DEPOSIT, TÜRKIYE

Keywords

barite, Batman, microthermometry measurements, REE geochemistry

Abstract

Orenagil barites are observed as space fillings, veins, and lenses incompatible with the host rock within the Devonian-aged Meydan formation belonging to the Bitlis metamorphics observed in the Bitlis suture zone in the north of Sason (Batman, Türkiye). Bitlis metamorphites are an important unit that hosts many mineral deposits. Since the study area is very close to the Bitlis suture zone, the effect of tectonism is intensely observed in the field. The mineral assemblage consists of barite, pyrite, chalcopyrite, hematite, goethite, magnetite, bornite, chalcocite, covellite, malachite, azurite, and limonite. The $BaSO_4$ content of barite samples ranges from 25 to 61 wt% and contains high SrO (2.04 wt%). Fluid inclusions observed in barite samples are predominantly of the fluid-rich two-phase (Liquid+Vapour) type. Homogenization temperatures of fluid inclusions in barites are observed in a wide range (169 to 382.1°C), and salinity values are collected in two different groups (0.27–6.9 wt% NaCl and 12.7–20.45 wt% NaCl). Eu/Eu* values (11.20–121.36) of barites indicate exhalative hydrothermal fluids, whereas Ce/La > 1 (10.03–54.76) indicates a terrestrial origin for barites. In spite of the average REE pattern of barite and their similar host rocks, barite differs from host rocks in terms of their negative Ce peak and strong positive Eu peak. The trends of the REE values of the samples and the values of the barites in the Ce_N/Sm_N–Ce_N/Yb_N diagram indicate that the barites are formed from multiple sources, including seawater and meteoric water.

GEOCHEMIA I MIKROTERMOMETRIA INKLUZYJNA W ZŁOŻU BARYTU ORENAGIL, TURCJA

Słowa kluczowe

baryt, Batman, pomiary mikrotermometryczne, geochemia REE

Streszczenie

Baryty Orenagil obserwuje się jako wypełnienia przestrzeni, żyły i soczewki niekompatybilne ze skałą macierzystą w obrębie formacji Meydan wiekowej dewonu, należącej do metamorfików Bitlis obserwowanych w strefie szwów Bitlis na północy Sason (Batman, Turcja). Metamorfity Bitlis są ważną jednostką, w której znajduje się wiele złóż minerałów. Ponieważ obszar badań znajduje się bardzo blisko strefy szwu Bitlisa, w terenie intensywnie obserwuje się wpływ tektonizmu. Zespół minerałów składa się z barytu, pirytu, chalkopirytu, hematytu, getytu, magnetytu, bornitu, chalkocytu, kowelinu, malachitu, azurytu i limonitu. Zawartość $BaSO_4$ w próbkach barytu waha się od 25 do 61% wag. i zawiera wysoką zawartość SrO (2,04% wag.). Wtrącenia płynne obserwowane w próbkach barytu

są głównie typu dwufazowego bogatego w płyn (ciecz + para). Temperatury homogenizacji wtrąceń płynnych w barytach obserwuje się w szerokim zakresie (169 do 382,1°C), a wartości zasolenia zbierane są w dwóch różnych grupach (0,27–6,9% wag. NaCl i 12,7–20,45% wag. NaCl). Wartości Eu/Eu* (11,20–121,36) barytów wskazują na ekshalacyjne płyny hydrotermalne, natomiast Ce/La > 1 (10,03–54,76) wskazują na ziemskie pochodzenie barytów. Pomimo średniego układu REE barytu i podobnych skał macierzystych, baryt różni się od skał macierzystych pod względem ujemnego piku Ce i silnego dodatniego piku Eu. Trendy wartości REE próbek i wartości barytów na wykresie Ce_N/Sm_N–Ce_N/Yb_N wskazują, że baryty powstają z wielu źródeł, w tym z wody morskiej i wody meteorycznej.